



## A DEDICATED LES EXPERIMENTAL DATABASE FOR THE ASSESSMENT OF LES SGS MODELS: THE PULSATILE JET IMPINGEMENT IN TURBULENT CROSS FLOW

**Hubert Baya Toda**

Energy Applications Techniques  
IFP Energie Nouvelles  
Rueil - Malmaison, France  
hubert.baya-toda@ifpen.fr

**Olivier Cabrit**

Department of Mechanical Engineering  
University of Melbourne  
Victoria 3010, Australia  
o.cabrit@unimelb.edu.au

**Karine Truffin**

Energy Applications Techniques  
IFP Energie Nouvelles  
Rueil - Malmaison, France  
karine.truffin@ifpen.fr

**Gilles Bruneaux**

Energy Applications Techniques  
IFP Energie Nouvelles  
Rueil - Malmaison, France  
gilles.bruneaux@ifpen.fr

**Franck Nicoud**

CNRS I3M 5149  
University Montpellier II  
Montpellier, France  
franck.nicoud@univ-montp2.fr

### ABSTRACT

In the present paper, a Large Eddy Simulation (LES)-dedicated experimental database is introduced for the assessment of Subgrid Scale (SGS) models in complex geometries. The experiment consists in a pulsatile impinging jet in presence of a turbulent cross flow. The configuration involves different flow features encountered in complex configurations: shear/rotating regions, stagnation point, wall-turbulence interaction as well as the propagation of a vortex ring on the impinging surface. The experiment was designed so as it is easily reproducible with LES and to allow the use of quantitative and non intrusive optical diagnostics. Measurements of velocity in different planes were performed using Particle Image Velocimetry (PIV). Some LES results using the dynamic Smagorinsky model (Germano et al., 1991) and the  $\sigma$ -model (Nicoud et al., 2011) are presented.

### 1 INTRODUCTION

Since the pioneer works of Smagorinsky (Smagorinsky, 1963) numerous SGS viscosity models (see Sagaut et al., 2009 for a comprehensive review) were developed but their extension to complex geometries such as Internal Combustion engines (IC engines) remains an open question. This is notably the case for the well known dynamic Smagorinsky model because the complexity of the flows involved in such configurations limits the possibility of averaging over homogeneous directions (combustion, spray atomization, multiphase flows, wall interaction...). Although different improvements (Ghosal et al, 1994, Meneveau et al., 1996) of the dynamic Smagorinsky model were developed, the lack of detailed and relevant experimental data dedicated to complex flows restricts the assessment of SGS viscosity models to academic test cases such as homogeneous isotropic turbulence and turbulent wall-bounded flows (Moser et al., 1999, Comte-Bellot and Corsin, 1971). Unfortunately, in IC engines for instance, turbulence is most

likely not isotropic, boundary layers are seldom established and are probably disturbed by the external flows. The alternative chosen in this work is to deal with a configuration which is simple enough to allow detailed understanding and control of the simulations and experimental measurements, but complex enough to capture/reproduce the important features and therefore provide a good validation platform. The unsteady interaction between vortices and their impingement with solid boundaries in a turbulent environment was chosen to this purpose. Figure 1 shows a schematic representation of the flow features from this experiment. PIV measurements were performed for measuring the velocity field. The experiment is characterized by the formation of a vortex ring followed by its impingement and propagation on the solid surface. LES simulations of the experimental set-up were also performed in order to assess performances of the dynamic Smagorinsky model (Germano et al., 1991) and the  $\sigma$ -model (Nicoud et al., 2011). These two models were selected because they both account for solid boundaries and vanish in various laminar flow configurations (pure shear, pure rotation, pure dilatation ...), the dynamic Smagorinsky model thanks to the dynamic procedure and the  $\sigma$ -model thanks to an advanced time scale operator. The objective of this work is then twofold: provide an experimental database for model validation purposes and assess performances of two SGS models already validated on academic test cases.

The present paper is organized as follows: in section II the design guidelines of the experiments are briefly recalled. The numerical set-up of the simulation of the experiment is presented in section II and in section IV velocity field comparisons between LES and PIV results are presented. As the present study focused on the velocity comparisons, it was decided not to linger on the details concerning the temperature measurements.

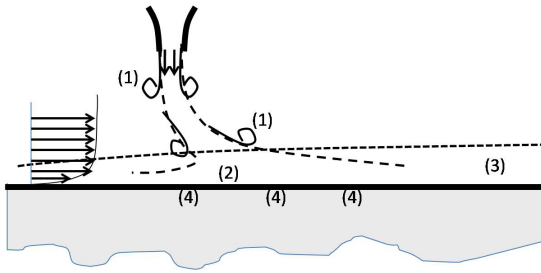


Figure 1. Flow features of the experimental set-up: (1) vortex roll up, (2) stagnation region, (3) shear and boundary layers, (4) heat transfer

## 2 EXPERIMENTAL APPARATUS AND DESIGN GUIDELINES

Among the aerothermal flow features encountered in IC engines, one of the most important is the wall impingement of the vaporized fuel jet on the piston head in a turbulent environment. The main objective during the design of the experimental apparatus was then to reproduce this feature in a more simple configuration. The flow pattern was simplified as a formation of vortices convected in a turbulent environment and finally impinging on a solid surface. Particular attention has been paid during the entire design phase to ensure that the dimensions (and consequently the Reynolds number) of the apparatus remain small enough to perform well resolved LES while staying sufficiently large to facilitate optical diagnostics measurements. The guidelines listed hereafter highlight the choices made during the design phase, to respect the constraints imposed by computational issues and those imposed by the need for easy optical access and accurate measurements:

**Dimensions and unsteadiness:** The distance  $H$  between the injector exit and the impingement surface is set to  $H = 2D$  (where  $D = 1$  cm is the diameter of the injector) in order to allow the formation of the vortex ring and to minimize the number of nodes that would be used during the simulations of the experiment.

**Low Mach number flows:** Most of the SGS viscosity models are developed in the framework of incompressible flows and are further extended to compressible flows (Sagaut et al., 2009) under the assumption of low Mach number. It typically means  $M \leq 0.2$  which corresponds in our case to a maximum value for the velocity around 80 and 95 m/s.

**Cross flow:** The velocity of the cross flow is monitored with a hot wire and tuned in order to have deviation of the jet of the order of the jet diameter. This was done by visualization at different cross flow rates using Schlieren visualization technique. The turbulent intensity of the cross flow is generated by a grid situated at 10 cm upstream of the jet inlet.

**Optical accessibility:** Wide optical accesses are provided by UV quality (Excimer 248 nm) large quartz windows in order to optimize the application of advanced optical diagnostics. The final experimental set-up is equipped with 4 wide optical accesses, two on the sides parallel to the cross flow, one perpendicular to the cross flow and another one on the top.

The injected gas is nitrogen and the inlet jet temperature is around 347 K. PIV measurements are performed using a doubled frequency Nd:YAG-laser at 532nm. The signal is recorded with a CCD camera of 2048 X 2048 pixels resolu-

tion. The time delay between the two pulses is 2  $\mu$ s. Measurements show the formation of a vortex ring, its impingement on the solid surface and its deviation at later injection times due to the cross flow.

## 3 Numerical Set-up

### 3.1 Solver and subgrid-scale models

The solver used during the entire study is AVBP ([www.cerfacs.fr/cfd/cfdpublications.html](http://www.cerfacs.fr/cfd/cfdpublications.html)). It is a parallel code that offers the possibility to handle structured or unstructured grids in order to solve the full 3D compressible reacting Navier-Stokes equations with a cell-vertex formulation. The efficiency and accuracy of the solver have been widely presented and demonstrated in academic and industrial configurations in the past years (Moureau et al., 2005). The resolved equations are the Favre filtered continuity, mass species conservation and compressible Navier-Stokes equations.

For sake of simplicity, emphasis is put only on the SGS viscosity models. Two SGS models are assessed on this experiment: the  $\sigma$ -model and the dynamic Smagorinsky model. Both account for flows variations, the first one through the time scale and the second through the dynamic procedure. Because the flow is 3D in the mean, averaging the dynamic constant over homogeneous direction (recommended practice when using the dynamic procedure), could not be used in the present work. A local spatial averaging was used instead, the remaining negative values of the dynamic Smagorinsky constant being clipped to zero to avoid stability issues. No averaging nor clipping was necessary for the  $\sigma$ -model. Indeed, its time scale is built so as to generate zero eddy-viscosity for any two-dimensional or two component flows, as well as for axisymmetric and isotropic compression/dilatation. Besides, it also has the proper cubic behavior in near wall regions and thus does not require any local dynamic procedure (Nicoud et al. 2011, Baya Toda et al. 2010)

### 3.2 Geometry simplification and mesh

The whole experimental apparatus is simulated with two simplifications (see Fig. 2): The injection system is not taken into consideration because the geometry of the injector is unknown. The grid for imposing the turbulence is not considered since the small size of the holes would reduce the solver time-step and increase the computational time. The computational domain starts downstream of the grid and the experimental mean and fluctuating velocity components are imposed as inlet boundary conditions. The length of the exhaust pipe is limited because the real dimensions are too large to be taken into account. Still, the simulated length is long enough to avoid any outflow difficulties due to the strong recirculating structure appearing in the chicane before the outlet. As in most CFD simulations, the resolution of the mesh plays an important role in the results quality, specially in LES simulations for which the size of the node volumes defines the filter cutoff. To this regard, a particular attention is paid on the mesh resolution near the wall and in the convergent volume. The computational domain contains 12.7 millions tetrahedral cells and 2.3 million nodes. The wall friction velocity  $u_\tau$  (before the impingement of the jet) for defining the mesh resolution at the wall is assessed from the Dean's correlation for a turbulent channel flow. The reference velocity is set to the maximum cross

flow velocity around 12 m/s. The size of the cells is chosen in order to have a mesh resolution of  $y^+ = \frac{\Delta y u_\tau}{\nu_w} \approx 4$  in the vicinity of the wall boundaries (where  $\nu_w$  is the kinematic viscosity at impinging surface temperature).

## 4 Experimental and Numerical results

### 4.1 Statistical analysis procedure

In order to reduce CPU time and similarly to the strategy used by Cabrit and Nicoud (2010), it was decided to perform independent LES with different uncorrelated initial conditions. In this way, there is no need to compute the 1 s delay between two consecutive injections as in the experiment. The two needed values for each individual LES simulations are the inlet flow rate and the cross flow. Concerning the former, the same inlet flow rate is used for all the individual simulations. This is justified by the large value of the mean inlet velocity. For the latter, a two steps strategy is adopted: the first step consists in starting with a cross flow generated by imposing a velocity field that match the cross flow in the experiment and to run the simulation with the injector switched off until the cross flow reaches a steady turbulent state under the injector. The time duration for this first step is estimated to be 50 ( $\approx 17 \frac{H}{u_c}$ ). Once the steady state is reached, the second step consists in saving individual solutions with a time interval of 10 ms (with the injector still switched off) which is considered sufficient to have uncorrelated turbulent cross flow solutions. Finally, the ensemble average is obtained from 10 LES.

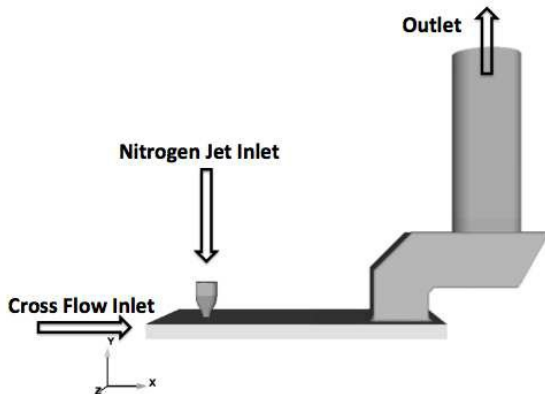


Figure 2. Geometry used for the simulation of the experimental set-up.

### 4.2 Velocity field comparisons

Figure 3 shows the general organization of the flow over time. A vortex ring is first created at the injector mouth (a) and propagated downwards. The large coherent vortex ring disintegrates when impacts the wall surface and structures of smallest size appears (b). At later instants, the injected flow rate decreases and the jet is deflected by the cross flow (d). Due to the important range of scales generated in this flow, it is anticipated that the numerical results could be sensitive to both the numerical scheme and the SGS model.

Before comparing the predictions of the different models, some preliminary tests were performed, to study the

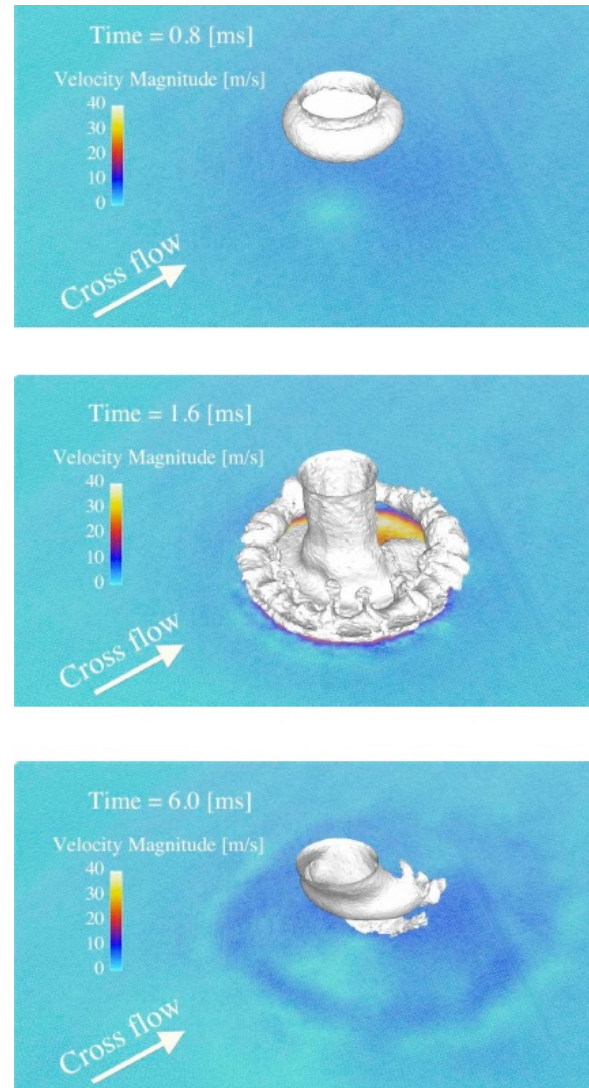


Figure 3. Sequence obtained from instantaneous LES fields showing the impact of the vortex-ring appearing at the beginning of the jet impulse. White iso-surface: temperature delimitating the hot region coming from the jet and the cold cross flow. Colored plane: velocity magnitude 1 mm above the flat plate.

influence of the statistical convergence of the PIV data, the numerical scheme and the number of solutions used for the ensemble average:

**Statistical convergence of the PIV data:** The objective was to ensure that the minimum number of snapshots (200) used during the experiments was sufficient to reach statistical convergence. It was observed a weak variation of the mean and rms velocity after 50 snapshots.

**Number of solutions used for averaging in LES simulations:** The ensemble average was performed over 10 LES simulations due to computational time costs. The objective of this test was to assess how the number of solutions can affect the results. Comparisons between one LES solution and 10 solutions using the Lax-Wendroff scheme and the SGS dynamic Smagorinsky model was performed. Little differences were observed during the first phase of the jet (for which the jet velocity is higher compare to the cross flow velocity) but some differences appear during the second phase for which the jet velocity is at the same order of

magnitude as the cross flow.

**Numerical scheme:** LES of academic cases are often performed with low dissipative schemes accurate in time which are generally not used for industrial applications. Two numerical schemes were tested using the same SGS model (the dynamic Smagorinsky model): The Galerkin (GRK) numerical scheme which is a centered finite element method, 4th order accurate in space with a 3<sup>rd</sup> order Runge-Kutta temporal integration. The Lax-Wendroff (LW) numerical scheme which is a finite volume numerical scheme 2<sup>nd</sup> order accurate in space with a single step integration. It has the advantage to be less CPU demanding than the GRK scheme. No major differences were observed when comparing results obtained with the two schemes. This result is obviously not general and strongly dependent on the configuration of interest and the quality of the spatial discretisation. On the other hand, the good agreement between LW and GRK results can also be seen as an indicator of the good quality of the mesh resolution used.

After the preliminary tests, the influence of the SGS viscosity model is investigated by comparing results from the  $\sigma$ -model and the dynamic Smagorinsky model. In both cases, results are averaged over 10 cycles and performed with the Lax-Wendroff-scheme. We will focus in this paper on 3 time of the experiment on the median plane: 1.2 ms during the impingement of the vortex ring on the bottom surface, 2.0 ms during the vortex propagation of the vortex ring along the bottom surface and 7.0 ms during the deviation of the jet by the cross flow. Actually the comparisons of results of the two models against experiment can be summarized in three phases:

**Vortex ring formation (0.8 - 1.2 ms):** It corresponds to the first timing during the formation of the vortex ring. During this phase the momentum flux ratio  $J = \frac{\rho_{jet}(V_{jet})^2}{\rho_{\infty}(V_{\infty})^2}$  is around 45 and the solid boundary has no impact on the flow. The end of this phase is when the vortex ring hits the wall. Predictions of the two models are similar and close to the experiment at it can be seen in Fig. 4(a)

**Vortex ring propagation (1.2 - 3.0 ms):** After the vortex ring hits the wall, it propagates along the solid boundary and first differences between model predictions are observed. Indeed, the velocity predictions of the vortex ring is under-predicted by the dynamic Smagorinsky whereas it is well reproduce with the  $\sigma$ -model as it can be seen in Fig. 4(b)

**Jet deviation (3.0 - 7.0 ms):** During this phase, the inlet velocity of the jet decreases and the momentum flux is of order of magnitude 0.5. The vortex ring is already dissipated and the jet is deviated by the cross flow. As in the first phase the solid boundary has almost no impact on the flow. Predictions of the two model are in good agreement with the experiment and the deviation of the jet is well predicted by the two model (see Fig. 4(c)).

Although, comparisons are limited in this paper to only three timing on the median plane, results on the other planes confirmed the precedent observations.

## 5 Discussions

In order to better understand the predictions of the mitigate results of the dynamic Smagorinsky model, it is important to recall some basics about the principle of the dynamic procedure, specially near solid boundaries. This procedure was developed to make the SGS dissipation consistent with the structure of the resolved flow and numerical discretisa-

tion. It also has the ability to accommodate the expected decrease of the SGS viscosity near solid walls with the large values of the strain rate induced by the no-slip condition. In other words, the prediction of the dynamic Smagorinsky model relies on the ability of the constant to vanish near solid walls following the well known  $y^{+3}$  near wall behavior. It should be stressed that the expected  $y^{+3}$  behavior corresponds to strong variations of  $C_s^2$  in the near wall region. Indeed, the Germano-identity reads:

$$T_{ij} - \widehat{\tau}_{ij} = L_{ij}, \quad (1)$$

where  $T_{ij}$  and  $\tau_{ij}$  are respectively the SGS shear stress at the test and initial filter level and  $L_{ij}$  is the modified Leonard term. Introducing the constant  $C_s^2$ , Eq. 1 reads:

$$C_s^2 \widehat{\Delta} \widehat{\mathcal{D}}_s \widehat{S}_{ij} - \Delta^2 (C_s^2 \widehat{\mathcal{D}}_s S_{ij}) = L_{ij} \quad (2)$$

In order to calculate  $C_s^2$  from Eq. 2, it is assumed that it can be removed from the test filter in the second term of the left hand side of the equation. The near wall behavior of the constant  $C_s^2$  is thus somehow in contradiction with the hypothesis of taking the constant out of the test filter. Let us consider for example a mesh with constant mesh spacing  $\Delta_y^+$  along the y-axis, at a node within the boundary layer situated at  $y^+$ . The theoretical behavior of the dynamic constant is  $C_s^2 \approx y^{+3}$ . It leads to a variation of the dynamic constant over the cell width which can be expressed as follows:

$$C_s^2(y^+ + \Delta_y^+) \sim C_s^2(y^+) + 3y^{+2}\Delta_y^+ + 3y^+\Delta_y^{+2} + \Delta_y^{+3}. \quad (3)$$

As  $\Delta_y^+$  is a fraction of the  $y^+$  position, the two last terms of the right hand side of the equation can be considered negligible and Eq. 3 reads:

$$C_s^2(y^+ + \Delta_y^+) \sim C_s^2(y^+)(1 + 3\frac{\Delta_y^+}{y^+}). \quad (4)$$

Eq. 4 shows that the grid spacing should be very small ( $\sim 1$ ) in order to minimize the systematic error  $3\frac{\Delta_y^+}{y^+}$  on the constant over the cell width. Assuming for example a 30% increase at the node  $y^+ = 10$ , the filter width should be of the order  $\Delta_y^+ \simeq \frac{10 \times 0.3}{3} \simeq 1$ . Such mesh requirements are affordable in academic configurations but can hardly be achieved in industrial applications for which  $\Delta_y^+ \sim 4 - 5$  is a common practice. In addition to the hypothesis of weak variation of the constant near solid boundaries that is not necessarily respected, there is another issue concerning the stabilization of the model constant. In the present case, a volume weight average method is performed for stabilization. It means that nodes that do not necessarily have the same strain rate intensity share the same average model constant for the damping. This procedure helps to stabilize the calculation but also affects the ability of the dynamic procedure to damp the turbulent viscosity near solid walls. Figure 5 shows the ratio of the SGS to molecular viscosity on the median plane in the streamwise direction during the impingement of the vortex ring on the wall and at

a late injection time. During the vortex impingement the SGS viscosity of the Smagorinsky model (see Fig. 5(a) to (c)) strongly increases compare to the  $\sigma$ -model which only weakly varied. The dynamic Smagorinsky model increases in the region where there is a strong gradient between the incoming velocity and the solid surface: at the stagnation point the SGS viscosity was weak but it increases at the vortex ring boundary. Very high values (and thus non physical) of SGS viscosity at wall nodes are even obtained as shown in Fig. 5(a,b). At late injection time (see Fig. 5(d)), there is no more increase of the dynamic Smagorinsky SGS viscosity. The velocity magnitude is low and more likely well resolved by the mesh so that the damping of the strain rate by the dynamic constant is successful. Concerning the  $\sigma$ -model, the fully local definition of the time scale (no explicit filtering or averaging needed) allows to automatically vanish near solid boundary as long as there are some nodes in the boundary layer. As a result the viscosity level remains very low during the entire injection phase even when the velocity gradient at the wall is high.

## 6 Conclusion

An experimental database of a pulsatile impinging hot jet in presence of a cold cross flow was presented in this paper. The experiment was designed so as to be tractable by LES. The boundary conditions were also well characterized. The inlet flow rate and the cross flow were characterized. PIV measurements were performed which showed that the experimental set-up reproduced several interesting flow features namely the formation of a vortex ring, its impingement and propagation along a solid wall followed by a deviation of the jet by the cross flow. The performances of two SGS viscosity models were assessed by performing LES of this experimental database. Comparisons focused on the velocity fields. The two tested models were the dynamic Smagorinsky model (Germano et al. 1991) (with a local formulation of the constant and clipping of negative values) and the  $\sigma$ -model (Nicoud et al. 2011, Baya Toda et al. 2010). The differences between the two models appeared during the interaction of the vortices with the bottom wall. During this phase, the propagation velocity of the vortices was under-predicted by the local dynamic Smagorinsky model. The authors suggest that it is due to an overestimation of the SGS viscosity during impingement leading to a too fast dissipation of vortices. At the same time, the  $\sigma$ -model which is based on invariants of the velocity gradient tensor automatically vanished on the bottom wall and led to a better prediction of the propagation velocity. The mitigate predictions of the dynamic Smagorinsky model were explained by different reasons: the model was not applied as recommended with a stabilization over homogeneous directions, the systematic clipping led to an over-estimation of the total SGS dissipation and finally the dynamic procedure was strongly dependent on the mesh resolution specially in the boundary layer. PIV results as well as the geometry and the mesh used for the LES are made available to the community upon request to the authors.

## REFERENCES

Germano, M. and Piomelli, U. and Moin, P. and Cabot, W. 1991 "A dynamic subgrid-scale eddy viscosity model",

Physics of Fluids, 3 1760-1765.

Nicoud, F., Baya Toda, H., Cabrit, O., Bose, S., Lee, J. 2011 "Using singular values to build a subgrid-scale model for Large Eddy Simulations", Physics of Fluids, 23.

H. B. Toda, O. Cabrit, G. Balarac, S. Bose, J. Lee, H. Choi, and F. Nicoud. 2010 "A subgrid-scale model based on singular values for LES in complex geometries". In NASA Ames/Stanford Univ. Center for Turbulence Research, editor, Proc. of the Summer Programm, pages 193202.

Smagorinsky, J. 1963 "General circulation experiments with the primitive equations", Month. Weather, 93, 99-165.

O. Metais and M. Lesieur. 1992 "Spectral large-eddy simulation of isotropic and stably stratified turbulence", Journal of Fluid Mechanich., 256:157194, 1992.

Comte-Bellot, G., Corsin, S. 1971 "Simple Eulerian time correlation of full narrow-band velocity signals in grid generated "isotropic" turbulence". Journal of Fluid Mechanics, 48, 273-337.

S. Ghosal, T.S. Lund, P. Moin, and W. H. Cabot. 1994 "A dynamic localization model for large-eddy simulation of turbulent flows", Journal of Fluid Mechanic, 282:127.

R. D. Moser, J. Kim, Manssour, N. N. 1999 "Direct numerical simulation of turbulent channel flow up to  $Re_\tau = 590$ ", Physics of fluids, 11(4).

P. Sagaut, E. Garnier, and N. Adams. 2009 "Large eddy simulation for compressible flows", Springer Science Science + Business Media B. V.

V. Moureau, G. Lartigue, Y. Sommerer, C. Angelberger, O. Colin, and T. Poinsot, 2005, "Numerical methods for unsteady compressible multi-component reacting flows on fixed and moving grids" Journal of Computational Physics, 202:710736.

O. Cabrit and F. Nicoud. 2010 "Direct numerical simulations of a reacting turbulent channel flow with thermo-chemical ablation". J. of Turbulence, 11(44):133.

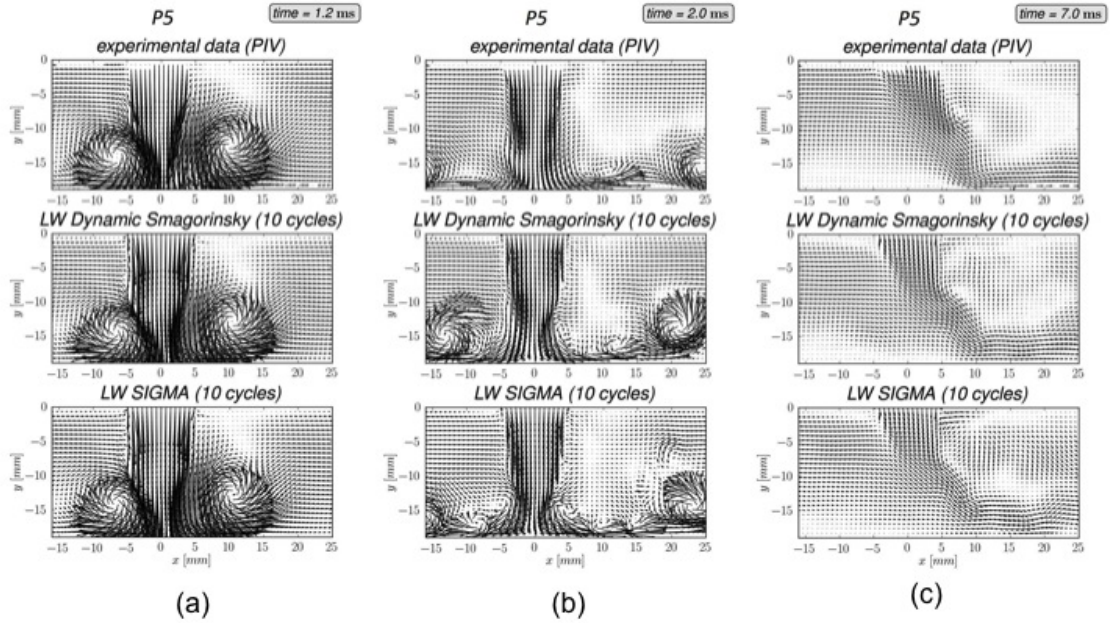


Figure 4. (a) Influence of the SGS viscosity model on the velocity field in the median plane (streamwise direction) at (a)  $t = 1.2$  ms (b)  $t = 2.0$  ms (c)  $t = 7.0$  ms.

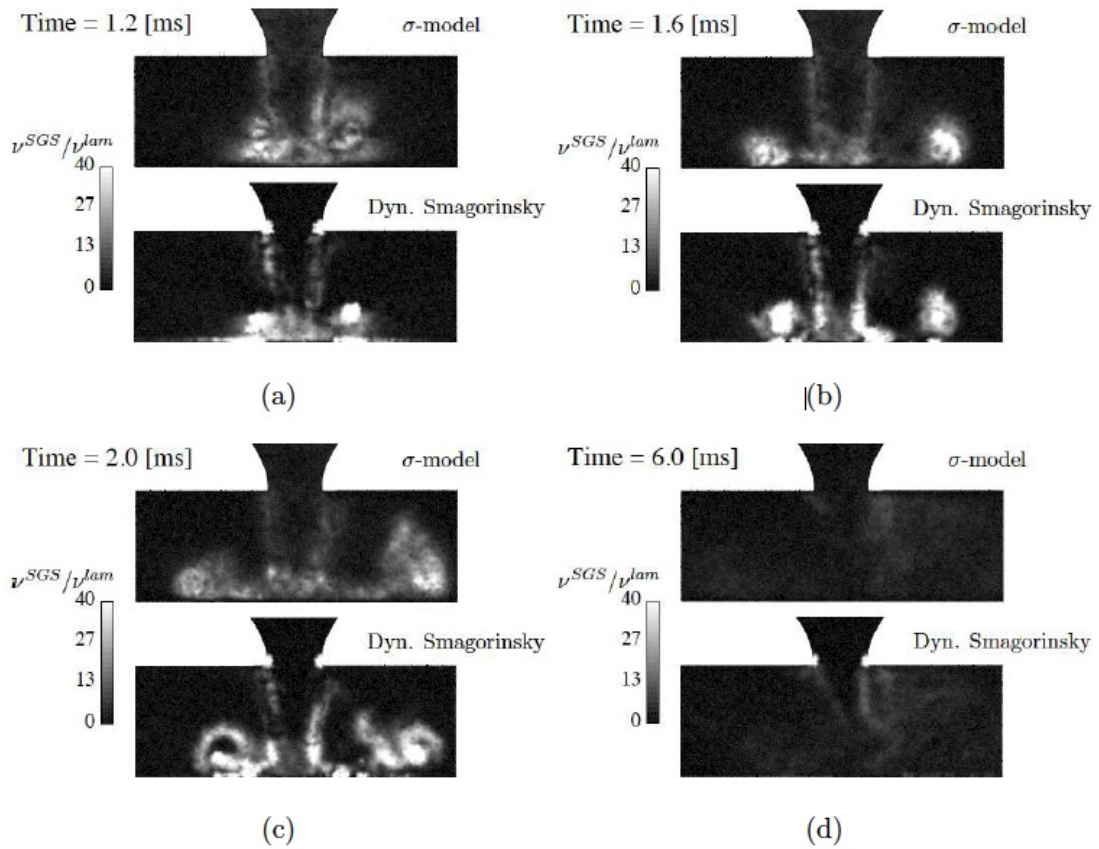


Figure 5. Field of the SGS to molecular viscosity ratio in in the median plane (streamwise direction) at (a)  $t = 1.2$  ms (b)  $t = 1.6$  ms (c)  $t = 2.0$  ms (d)  $t = 6.0$  ms.